HHS Public Access

Author manuscript

J Mol Biol. Author manuscript; available in PMC 2024 May 13.

Published in final edited form as:

J Mol Biol. 2024 February 15; 436(4): 168410. doi:10.1016/j.jmb.2023.168410.

Impact of polβ/XRCC1 Interaction Variants on the Efficiency of Nick Sealing by DNA Ligase IIIα in the Base Excision Repair Pathway

Danah Almohdar[1], **Mitchell Gulkis**[1], **Abigail Ortiz**[1], **Qun Tang**[1], **Robert W. Sobol**[2], **Melike Çağlayan**[1]

[1]Department of Biochemistry and Molecular Biology, University of Florida, Gainesville, FL 32610, USA

[2]Department of Pathology and Laboratory Medicine, Warren Alpert Medical School & Legorreta Cancer Center, Brown University, Providence, RI 02912, USA

Abstract

Base excision repair (BER) requires a coordination from gap filling by DNA polymerase (pol) β to subsequent nick sealing by DNA ligase (LIG) IIIα at downstream steps of the repair pathway. X-ray cross-complementing protein 1 (XRCC1), a non-enzymatic scaffolding protein, forms repair complexes with polβ and LIGIIIα. Yet, the impact of the polβ mutations that affect XRCC1 interaction and protein stability on the repair pathway coordination during nick sealing by LIGIIIα remains unknown. Our results show that the polβ colon cancer-associated variant T304 exhibits a reduced interaction with XRCC1 and the mutations in the interaction interface of V303 loop (L301R/V303R/V306R) and at the lysine residues (K206A/K244A) that prevent ubiquitin-mediated degradation of the protein exhibit a diminished repair protein complex formation with XRCC1. Furthermore, we demonstrate no significant effect on gap and nick DNA binding affinity of wild-type polβ by these mutations. Finally, our results reveal that XRCC1 leads to an efficient channeling of nick repair products after nucleotide incorporation by polβ variants to LIGIIIα, which is compromised by the L301R/V303R/V306R and K206A/K244A mutations. Overall, our findings provide insight into how the mutations in the polβ/XRCC1 interface and the regions affecting protein stability could dictate accurate BER pathway coordination at the downstream steps involving nick sealing by LIGIIIα.

Correspondence to Melike Çağlayan: caglayanm@ufl.edu (M. Çağlayan).

Edited by M Gottesman

CRediT authorship contribution statement

Danah Almohdar: Data curation, Formal analysis, Investigation, Methodology, Validation, Visualization, Writing – original draft, Writing – review & editing. **Mitchell Gulkis:** Formal analysis, Investigation, Methodology, Validation, Writing – original draft. **Abigail Ortiz:** Investigation, Writing – review & editing. **Qun Tang:** Investigation, Validation. **Robert W. Sobol:** Funding acquisition, Resources, Writing – review & editing. **Melike Çağlayan:** Conceptualization, Funding acquisition, Supervision, Writing – original draft, Writing – review & editing.

DECLARATION OF COMPETING INTEREST

The authors declare the following financial interests/personal relationships which may be considered as potential competing interests: RWS is co-founder of Canal House Biosciences, LLC, is on the Scientific Advisory Board, and has an equity interest. The authors declare no competing interests.

Appendix A. Supplementary data

Supplementary data to this article can be found online at https://doi.org/10.1016/j.jmb.2023.168410.

Keywords

base excision repair; DNA polymerase β; DNA ligase IIIα; X-ray cross-complementing protein 1; repair pathway coordination

Introduction

Base excision repair (BER) is the primary repair pathway that deals with small, non-helix-distorting lesions such as base oxidation or alkylation, abasic (AP) sites, and single-strand breaks.[1–3] The BER pathway is the multi-enzyme mechanism that involves processing of the repair intermediates between the core repair proteins in an orderly fashion.[4–6] DNA damage-specific DNA glycosylase first recognizes and removes a single-base lesion through hydrolysis of the N-glycosidic bond, creating an abasic site in the double-stranded DNA.[7,8] AP endonuclease 1 (APE1) then cleaves the phosphodiester backbone at the AP-site, leaving a 5'-deoxyribosephosphate (dRP) at the terminus that is removed in the next step by DNA polymerase (pol) β.[9] During the downstream steps of the BER pathway, polβ performs template-directed gap filling DNA synthesis, which results in generation of a nick repair intermediate for DNA ligase I or DNA ligase (LIG) IIIα that catalyze a phosphodiester bond formation between adjacent 3'-OH and 5'-P termini in the final step to complete the BER process.[10] The BER pathway involves the mechanism of the substrate-product channeling, also referred to as "passing-the-baton", which requires a tight coordination between the core repair proteins and the recognition of the enzyme-product complex by the next enzyme in the pathway to be used as a substrate for the next step.[11–14] This coordination is regulated through protein–protein and protein-DNA interactions. This prevents the release and accumulation of toxic and mutagenic single-strand break intermediates that could trigger cell cycle arrest, apoptosis, and harmful nuclease or recombination activities.[15–18] Yet, it is still unclear how a multi-protein/DNA complex functions to promote a larger protein assembly that can facilitate the channeling of repair intermediates in response to DNA damage.[19,20]

In addition to the core enzymes, the non-enzymatic accessory repair factors, such as scaffolding protein X-ray cross complementation protein 1 (XRCC1), play critical roles in assembling enzymes to promote the repair process and minimizing the release of labile repair intermediates.[21,22] XRCC1 interacts with multiple repair proteins through N-terminal domain (NTD), a central BRCT domain (BRCT-I), and a second BRCT domain (BRCT-II); and is recruited to DNA damage via its interaction with the initial BER enzymes that recognize and bind to a specific DNA lesion in the genome.[23–27] Its interactions with downstream BER enzymes polβ and LIGIIIα are mediated by NTD and BRCT-II domains, respectively.[28–32] Particularly, the hydrophobic region spanning residues F67 to V86 that reside in the NTD domain of XRCC1 is responsible for its interaction with polβ, and the string of nine amino acids, namely the V303 loop residing in dNTP selection sub-domain of polβ, has been identified as an interaction interface with XRCC1.[29–32] Although the biological significance of XRCC1 in the maintenance of genome integrity has been well reported, it is still not elucidated thoroughly at the biochemical level that how this scaffolding factor coordinates the repair process through protein–protein interactions

with polβ and LIGIIIα during the downstream steps of the BER pathway. In our previous study,[33] we demonstrated that polβ/XRCC1 complex increases the processivity of the BER reaction after nucleotide incorporation into the gap DNA by polβ and enhances the hand off resulting nick repair product to the final ligation step by LIGIIIα. Furthermore, we reported that XRCC1 cancer-associated variants (P161L, R194W, R280H, R399Q, Y576S) exhibit slight or no effect on protein–protein interactions with BER proteins polβ, Aprataxin, and LIGIIIα.

The tight interaction between XRCC1 and polβ is required for recruitment of the repair complex to the site of DNA damage, and modulates chromatin localization of the polymerase.[34–38] XRCC1 plays a role for subcellular localization of polβ and regulates its stability via the ubiquitin-dependent pathway, which is mediated by the lysine residues K206 and K244 residing in the C-terminal region of the protein.[39] polβ colon cancer-associated variant T304I and the mutations residing in the V303 loop (L301R/V303R/V306R) have been found to be associated with an increased level of polβ ubiquitylation, indicating that they may not be scaffolded by XRCC1 properly during BER.[40] Furthermore, when the single T304I mutation was combined with the mutations at the lysine residues K206A/K244A, the resulting triple mutant T304I/K206A/K244A was found to have increased rates of ubiquitin-independent degradation.[38–40] These previously reported findings suggest that the polβ/XRCC1 repair complex plays a key role in protecting polβ from ubiquitin-mediated degradation. Yet, the impact of the polβ mutations residing in this critical protein interaction interface and the residues that are important for stability of the polymerase on the BER repair pathway coordination scaffolded by XRCC1 during LIGIIIα activity at the downstream steps remains unknown.

In this study, we examined polβ colon cancer-associated variant T304I, the ubiquitylation mutants K206A/K244A, and V303 loop mutants L301R/V303R/V306R using a combined approach involving the protein complex formation through size-exclusion chromatography, GST-pull down assays, protein–protein interactions, and DNA binding measurements in real time as well as the repair assays to measure polβ gap filling coupled to nick sealing by LIGIIIα *in vitro*. Our results demonstrated that the polβ L301R/V303R/V306R triple mutant exhibits a diminished interaction and significant effect on the equilibrium binding constants (K*D*) of protein–protein interaction kinetics with XRCC1 in comparison with wild-type polβ. Furthemore, this triple-mutant has an inability to form a repair protein complex with XRCC1, while cancer-associated T304I variant shows a reduced, but not abolished, interaction with the scaffolding protein. Although there was no difference in gap and nick DNA binding affinity of the polβ wild-type, the variants carrying mutations in the XRCC1 interaction interface were able to perform mismatch insertions with higher efficiency than that of wild-type enzyme. Finally, our results demonstrated that the nick repair product after dGTP:C and 8oxodGTP:A insertions by the polβ variants carrying mutations at both the ubiquitiylation site (K206 and K244) and the V303 loop (L301R/V303R/V306R) cannot be efficiently sealed by LIGIIIα, which leads to the formation of ligation failure products and deleterious repair intermediates. Our overall findings revealed the molecular determinants that dictate BER accuracy and the importance of functional interplay and protein–protein interactions between downstream proteins polβ and LIGIIIα, particularly in the context of repair pathway coordination scaffolded by XRCC1.

Materials and Methods

DNA polymerase β constructs

Plasmid DNA constructs of full-length (1–335 amino acids) of DNA polymerase (pol) β mutants (pGEX-4 T-3) were confirmed by DNA sequencing prior to use. Polβ mutants are referred as following: T304I (SM), K206A/K244A (DM), T304I/K206A/K244A (TM1), L301R/V303R/V306R (TM2), and L301R/V303R/V306RK206A/K244A (DM/TM) as listed in Supplementary Table 1.

Protein purifications

Human full-length DNA polymerase (pol) β proteins (wild-type and mutants) with a GST-tag were overexpressed in BL21(DE3) *E.coli* cells in Lysogeny Broth (LB) media at 37 °C for 8 h and induced with 0.5 mM isopropyl β-D-thiogalactoside (IPTG) when OD_{600} reached to 0.8–1.0 as described previously.[41–45] The cells were then grown overnight at 28 °C and the cell lysis was obtained at 4 °C by sonication in the lysis buffer containing 1X PBS (pH 7.3), 200 mM NaCl, 1 mM DTT, and complete protease inhibitor cocktail. The cell lysate was pelleted at 16,000 x rpm for 1.5 hr and then clarified by centrifugation and filtration. The supernatant was loaded onto a GSTrap HP column and purified with the elution buffer containing 50 mM Tris-HCl (pH 8.0) and 10 mM reduced glutathione. In order to cleave the GST-tag of polβ proteins, the recombinant protein was incubated with a TEV protease for 16 hr at 4 °C in the buffer containing 1X PBS (pH 7.3), 200 mM NaCl, and 1 mM DTT. After the cleavage, the polβ protein was subsequently passed through a GSTrap HP column, and collected in the flowthrough. Polβ proteins were then further purified by Superdex 200 increase 10/300 column in the buffer containing 50 mM Tris-HCl (pH 7.5), and 400 mM NaCl. Polβ wild-type and mutants with and without GST-tag were overexpressed and purified similarly and the final purity of the proteins was presented in Supplementary Figure 1.

Human wild-type full-length (1–922 amino acids) DNA ligase (LIG) IIIα (pET-29a) with 6x-his tag was overexpressed in BL21(DE3) *E.coli* cells in LB media at 37 °C for 8 hr and induced with 0.5 mM IPTG as described.[41–45] The protein over-expression was continued overnight at 28 °C. The cells were harvested, lysed at 4 °C, and then clarified as described above. LIGIIIα protein was purified by a HisTrap HP column with an increasing imidazole gradient (20–300 mM) elution at 4 °C. The collected fractions were then further purified by Superdex 200 increase 10/300 column in the buffer containing 50 mM Tris-HCl (pH 7.0), 500 mM NaCl, glycerol 5%, 1 mM DTT. Human full-length (1–633 amino acids) XRCC1 wild-type and XRCC1/polβ interaction mutant V86R (pET-24b) with 6x-his tag were overexpressed in BL21 (DE3) *E.coli* cells in LB media with 100 μg/ml of kanamycin at 37 °C for 8 hr as described.[41–45] The cells were harvested, lysed at 4 °C, and then clarified as described above. XRCC1 proteins were purified by a HisTrap HP column with an increasing imidazole gradient (20–300 mM) elution at 4 °C, and the collected fractions were then loaded onto a HiTrap Heparin column in the binding buffer containing 50 mM Tris-HCl (pH 7.0), 50 mM NaCl, 1.0 mM EDTA, and 10% glycerol. The recombinant XRCC1 proteins were eluted with a linear gradient of NaCl up to 1 M, and then were further purified by Superdex 200 increase 10/300 column in the buffer containing 20 mM Tris-HCl

(pH 7.0), 200 mM NaCl, and 1 mM DTT. All proteins used in this study were analyzed on 10% SDS-PAGE, dialyzed against storage buffer containing 25 mM TrisHCl, pH 7.4, 100 mM KCl, 1 mM TCEP, and 10% glycerol, concentrated, frozen in liquid nitrogen, and stored at −80 °C in aliquots.

Size exclusion chromatography of polβ/XRCC1 protein complexes

The protein complex formation between polβ (wild-type and mutants) and XRCC1 (wild-type and polβ interaction mutant V86R) were obtained using size-exclusion chromatography (SEC) as described.[33] Briefly, polβ (5 μM) and XRCC1 (5 μM) were prepared at equimolar 1:1 ratio of both proteins in the buffer containing 50 mM Tris-HCl (pH 8.0), 200 mM NaCl, and 1 mM DTT. The protein complexes were incubated for 2 hr on ice and SEC was performed using Superdex 200 increase GL 10/30 column in the same buffer in which the protein complexes were made. The fractions corresponding to the peaks were collected and analyzed for shifts in individual protein (polβ or XRCC1) *versus* the BER protein complex (polβ/XRCC1) as elution volumes. The fractions corresponding to the elution peaks were collected and analyzed on 12% SDS-PAGE and the gels were scanned by AI680 (Amersham RGB). SEC experiments were performed similarly for polβ wild-type and mutants T304I (SM), K206A/K244A (DM), T304I/K206A/K244A (TM1), L301R/V303R/V306R (TM2), and L301R/V303R/V306RK206A/K244A (DM/TM).

BioLayer Interferometry assays for DNA binding measurements

We analyzed gap and nick DNA binding kinetics of polβ (wild-type and mutants) by BioLayer Interferometry (BLI) assays in real time using the Octet QKe system (Fortebio) as described.[33] BLI experiments were performed at 20 °C in 96-well microplates with agitation set to 1000 rpm in the absence and presence of gap or nick DNA substrates with 3'-biotin label. Streptavidin (SA) biosensors (Fortebio) were used to attach the biotin-labeled DNA. The SA biosensors were hydrated in the kinetics buffer containing 20 mM HEPES (pH 7.4), 200 mM NaCl, 0.5% BSA, 0.05% Tween 20 at 20 °C for 20 min. The sensors were then immersed in gap or nick DNA (40 nM) in the kinetics buffer for 300 s. After recording an initial baseline in the kinetics buffer (60 s), the sensors with DNA were exposed to polβ at the concentration range as indicated in the figure legends for 240 s association, and then in the kinetics buffer for 240 s dissociation. In all measurements, the affinity constants (K_D), the association (k_{on}) and dissociation (k_{off}) rates were calculated using the ForteBio Data Analysis software with 1:1 binding model. The association rate = k_{on} [ligand][analyte] and the dissociation rate = k_{off} [ligand-analyte]. At equilibrium, forward and reverse rates are equal. All images were drawn using Graph Pad Prism 9. BLI assays were performed using polβ proteins without a GST-tag and the affinity constants were measured similarly for polβ wild-type and mutants T304I (SM), K206A/K244A (DM), T304I/K206A/K244A (TM1), L301R/V303R/V306R (TM2), and L301R/V303R/V306RK206A/K244A (DM/TM).

Surface plasmon resonance assay for polβ/XRCC1 protein interaction measurements

We analyzed the protein–protein interactions between polβ (wild-type and mutants) and XRCC1 (wild-type and polβ interaction mutant V86R) by Surface Plasmon Resonance (SPR) in real time at 25 °C as described.[33] One flow cell of the CM5 sensor chip was activated with a 1:1 mixture of 0.2 M EDC and 0.05 M NHS in water, and then GST-tag

polβ protein was injected over the flow cell in 10 mM sodium acetate, at pH 5.0 at a flow rate of 10 μl/min. The binding sites were blocked using 1 M ethanolamine (pH 8.5). XRCC1 protein ranging in the concentrations as indicated in the figure legends were then injected for 240 s at a flow rate of 30 μl/min. The running buffer was the same as the protein storage buffer containing 10 mM HEPES (pH 7.4), 150 mM NaCl, 3 mM EDTA and 0.005% (v/v) Surfactant P20. After a dissociation phase for 240 s, 0.25% SDS was injected for 60 s to regenerate the chip surface. Non-specific binding to a blank flow cell was subtracted to obtain corrected sensorgrams. All data were analyzed using BIAevaluation software version 2.0.1 and fitted to a 1:1 (Langmuir) binding model to obtain equilibrium constants (K*D*) for polβ/XRCC1 interaction. The protein–protein interaction measurements were performed similarly for polβ wild-type and mutants T304I (SM), K206A/K244A (DM), T304I/K206A/K244A (TM1), L301R/V303R/V306R (TM2), and L301R/V303R/V306RK206A/K244A (DM/TM).

GST-pull down assays

GST-pull down assays were performed to validate the protein binding characteristics of polβ (wild-type and mutants) with XRCC1 (wild-type and polβ interaction mutant V86R) as described.[33] His-tag XRCC1 (5 μM) was first incubated with GST-tag polβ (5 μM) in the reaction buffer containing 50 mM Tris-HCl pH 7.5, 100 mM NaCl, 1 mM DTT at 4 °C for 2 h. As a control, the interaction of GST (5 μM) with wild-type XRCC1 (10 μM) was also examined. Proteins were then mixed with 20 μl of glutathione sepharose beads that were washed via centrifugation at 600 x g for 1 min a total of 3-times with water and 3-times with 1X PBS. The samples with the beads were then incubated with constant rotation at 4 °C for 2 h. The beads were washed and centrifuged at 600 x g for 1 min for a total of five times with the elution buffer containing 50 mM Tris-HCl (pH 8.0) and 10 mM reduced glutathione. The eluted protein samples were analyzed on 12% SDS-PAGE and the gels were scanned by AI680 RGB (Amersham). GST-pull down assays were performed similarly for polβ wild-type and mutants T304I (SM), K206A/K244A (DM), T304I/K206A/K244A (TM1), L301R/V303R/V306R (TM2), and L301R/V303R/V306RK206A/K244A (DM/TM).

Thermal stability assays

Thermal stability assays were conducted in 96 well plates using the CFX96 RT-PCR detection system (Bio-Rad). The experiments were performed in a reaction mixture containing polβ (1 μM) alone, or polβ (1 μM) in the presence of gap DNA (10 μM), in a total volume of 25 μl. Polβ was incubated with either water or gap DNA at 4 ° C for 1 hr, then Sypro Orange protein dye (Invitrogen) was added to a final concentration of 4X. The plate was then sealed with an optical seal and centrifuged. The thermal scan to measure protein denaturing ranged from 10–95 °C with a temperature ramp rate of 1 °C/min. The fluorescence intensity upon binding of Sypro Orange was measured with an excitation/emission of 533/580 nm. Data analysis and report generation was performed using the Maestro instrument software (Biorad). T_m values were calculated manually from the negative derivative plot at the point of inflection of the curve (the midpoint for protein unfolding). All images were drawn using Graph Pad Prism 9. Thermal shift assays were performed similarly for polβ wild-type and mutants T304I (SM), K206A/K244A

(DM), T304I/K206A/K244A (TM1), L301R/V303R/V306R (TM2), and L301R/V303R/V306RK206A/K244A (DM/TM).

Polβ nucleotide insertion assays

We investigated the effect of polβ mutations on the gap filling efficiency of the wild-type enzyme using one nucleotide gap DNA substrates (Supplementary Table 2) in the nucleotide insertion assays as described.[41–45] For this purpose, we tested correct (dGTP:C), mismatches (dATP:C, dTTP:C, dCTP:C, dATP:G, dTTP:G, dGTP:G), and oxidized nucleotide (8oxodGTP:A) insertions by polβ wild-type *versus* the mutants. The reaction mixture contains 50 mM Tris-HCl (pH 7.5), 100 mM KCl, 10 mM $MgCl_2$, 1 mM ATP, 1 mM DTT, 100 μgml^{-1} BSA, 10% glycerol, dNTP (dATP, dTTP, dGTP, dCTP) or 8-oxodGTP (100 μM), and DNA substrate (500 nM) in a final volume of 10 μl. The reaction was initiated by the addition of the polβ (10 nM) and the reaction mixtures were incubated at 37 °C for the time points as indicated in the figure legends. The reaction products were then mixed with an equal amount of gel loading buffer containing 95% formamide, 20 mM EDTA, 0.02% bromophenol blue, and 0.02% xylene cyanol, and separated by electrophoresis on an 18% polyacrylamide gel. The gels were finally scanned with a Typhoon PhosphorImager RGB (Amersham), and the data were analyzed using ImageQuant software. The nucleotide insertion assays were performed similarly for polβ wild-type and mutants T304I (SM), K206A/K244A (DM), T304I/K206A/K244A (TM1), L301R/V303R/V306R (TM2), and L301R/V303R/V306RK206A/K244A (DM/TM).

Polβ nucleotide insertion coupled to DNA ligation assays

We investigated the effect of SM, DM, TM1, TM2, and DM/TM mutations on the ligation of polβ nucleotide insertion products in the same reaction mixture using one nucleotide gap DNA substrates (Supplementary Table 3) as described.[41–45] We tested the ligation of correct dGTP:C insertion products in the reaction mixture including polβ and LIGIIIα in the absence and presence of XRCC1. Furthermore, we analyzed SM and TM2 mutants to test the efficiency of ligation by LIGIIIα after polβ oxidized nucleotide 8-oxodGTP:A insertions in the coupled assays. The reaction mixture contains 50 mM Tris-HCl (pH 7.5), 100 mM KCl, 10 mM $MgCl_2$, 1 mM ATP, 1 mM DTT, 100 μgml^{-1} BSA, 10% glycerol, dNTP or 8-oxodGTP (100 μM), and DNA substrate (500 nM) in a total volume of 10 μl. The reaction was initiated by the addition of a pre-incubated enzyme mixture of polβ/LIGIIIα or polβ/LIGIIIα in the presence of XRCC1. The reaction mixtures were incubated at 37 °C for the time points as indicated in the figure legends. The reaction products were then mixed with an equal amount of gel loading buffer and separated by electrophoresis on an 18% polyacrylamide gel. The gels were finally scanned, and the data were analyzed as described above. The coupled assays were performed similarly for polβ wild-type and mutants T304I (SM), K206A/K244A (DM), T304I/K206A/K244A (TM1), L301R/V303R/V306R (TM2), and L301R/V303R/V306RK206A/K244A (DM/TM).

Structure modelling of polβ variants

The structure modeling of polβ mutants was performed based on the previously solved crystal structures of polβ/gap DNA (PDB:1BPY) and polβ C-terminal/XRCC1 N-terminal (PDB:3K75). All structural images were drawn using PyMOL (https://www.pymol.org/).

Results

Protein complex formation of XRCC1/polβ variants

Polβ mutations, referenced through the present study as following T304I (SM), K206A/K244A (DM), T304I/K206A/K244A (TM1), L301R/V303R/V306R (TM2), and L301R/V303R/V306RK206A/K244A (DM/TM), reside in the DNA synthesis (149–262 amino acids) and dNTP selection subdomain (262–335 amino acids) within the polymerase domain of the protein (Figure 1 and Supplementary Table 1).

We first investigated the protein complex formation between polβ variants and XRCC1 through the size exclusion chromatography (SEC). For individual proteins, our SEC analyses demonstrated the elution peaks for polβ (wild-type and mutants) and XRCC1 (wild-type and V86R mutant) at 15.7 and 11.8 ml, respectively (Figure 2). In the control experiment, we showed protein complex formation comprised of wild-type polβ and XRCC1 (Figure 3A). Our SEC analysis of polβ variants T304I (SM), K206A/K244A (DM), and T304I/K206A/K244A (TM1) showed similar complex formation with XRCC1, which was co-eluted at 11.2 ml when these two proteins were mixed together (Figure 3A-C). There was a slight difference in the elution shifts between the polβ variants SM, DM, and TM1. In the another control experiment, we showed a lack of protein complex formation between polβ and XRCC1 mutant V86R, as both proteins eluted separately with no shift evident in their individual elution volumes (Figure 3D). Similarly, our SEC analysis of polβ variants L301R/V303R/V306R (TM2) and L301R/V303R/V306RK206A/K244A (DM/TM) demonstrated no protein complex formation with wild-type XRCC1 as shown in the elution peak positions separately at 11.6 and 15.7 ml (Figure 3E). These results demonstrate the BER complex of polβ/XRCC1 formation is affected by a combined effect of the mutations residing in the interaction interface and stability of polβ protein, which could interfere with the scaffolding role of XRCC1 for the recruitment of the polymerase to the side of damage for efficient BER.

Protein interaction kinetics of polβ variants with XRCC1

We then quantitatively monitored the kinetics of protein–protein interactions between XRCC1 and polβ variants using SPR assays where the GST-tag polβ protein was immobilized on CM5 biosensors onto which his-tag XRCC1 was respectively passed as analytes (Figure 4).

We observed a tight interaction between polβ and XRCC1 for wild-type proteins (K_D: 6.7 nM) and a significantly reduced equilibrium dissociation constant (K_D: 2.7×10^3 nM) for XRCC1 mutant V86R that is deficient in interaction with polβ (Supplementary Figure 2). In comparison with wild-type proteins, there was ~6-fold difference in the K_D between XRCC1 and polβ cancer-associated mutant T304I (Figure 4A). Similarly, polβ TM1 mutant harboring T304I, K206A, and K244A mutations showed a relatively weak interaction with K_D: ~45 nM (Figure 4B). Our results showed that polβ DM mutant carrying K206A and K244A mutations that reside in DNA synthesis domain of the protein has similar interaction profile (K_D: ~11 nM) with that of wild-type polβ and XRCC1 (Figure 4C). For the polβ mutants TM2 and DM/TM, we observed no interaction with XRCC1 (Figure 4D,E). Despite

using a concentration range of XRCC1 that is significantly higher than the concentration range used for the rest of the mutants, we were not able to measure the K_D for these polβ mutants carrying the triple V303 loop mutations (Figure 4F).

Effect of polβ variants on the binding efficiency to XRCC1

To further investigate the impact of polβ mutations on its interaction with XRCC1, we investigated polβ/XRCC1 binding by GST pull-down assays where GST-tag polβ (wild-type or mutants) was respectively incubated with his-tag XRCC1 (wild-type or polβ interaction mutant V86R). We first incubated the protein mixture to enable the protein–protein interaction between polβ and XRCC1 to occur and before being precipitated by GST-binding glutathione beads. The bound material was then captured in three independent experimental GST-pull down assays and analyzed on SDS-PAGE (Supplementary Figure 3).

We showed that the polβ T304I mutant exhibits reduced binding to XRCC1 (Supplementary Figure 3A, lanes 6 *versus* 9), while polβ double-mutant (DM, K206A/K244A) shows similar XRCC1 binding ability in comparison with wild-type proteins under the same reaction conditions (Supplementary Figure 3B, lanes 7 *versus* 10). We also demonstrated that the triple-mutant (TM1, T304I/K206A/K244A) exhibits a reduced interaction, which was found to be similar to the interaction between that of polβ T304I and XRCC1 (Supplementary Figure 3B, lanes 7 *versus* 11). Our results revelaled the most dramatic effect for the triple V303 mutants, TM2 (L301R/V303R/V306R) and DM/TM (K206A/K244A/L301R/V303R/V306R), where we obtained no complex formation with XRCC1 (Supplementary Figure 3C, lanes 5 *versus* lanes 10 and 11). This result was found to be similar with the negative control including wild-type polβ and XRCC1/polβ interaction-deficient mutant V86R. Overall, these findings for polβ wild-type *versus* variants were further validated the significant effect of the mutations located in the V303 loop region at the dNTP subdomain of the protein and their impact on abolishing XRCC1 interaction and protein complex formation.

Gap and nick DNA binding affinities of polβ variants

Using Biolayer Interferometry assays, we examined polβ variants to understand the impact of the mutations residing in XRCC1 interaction interface and the region that governs the protein stability on DNA binding efficiency of wild-type polβ. For this purpose, we used one nucleotide gap DNA that mimics the BER intermediate that polβ uses to insert a single nucleotide during the DNA synthesis step and nick DNA that represents polβ nucleotide insertion product being used by DNA ligase for ligation in the next and final step of BER pathway. Our results demonstrate that polβ binds to a gap DNA substrate with K_D: ~5 nM (Supplementary Figure 4A) and polβ variants exhibit similar DNA binding affinity (Figure 5). We showed the equilibrium binding constant values between 3.5–4.5 nM for all five polβ variants tested in this study (Figure 5A-E). Furthermore, our nick DNA binding measurement by wild-type polβ indicates ~4-fold weaker binding affinity (K_D: ~20 nM) than that of gap DNA binding (Supplementary Figure 4B). There was no drastic difference between all five polβ variants that exhibit the equilibrium binding constant values between ~14–23 nM (Figure 6). We only obtained the lowest nick DNA binding affinity (K_D: 30 nM) by polβ DM mutant carrying K206A and K244A mutations that reside in DNA synthesis domain of the protein and impact the protein stability (Figure 6B). Our overall gap and nick

DNA binding results demonstrate that the mutations that affect protein complex formation and interaction with XRCC1 can bind to the both repair intermediates with similar affinity and do not affect DNA binding ability of wild-type protein (Figures 5F and 6F).

Impact of polβ mutations on protein stability and folding

We evaluated the effect of polβ mutations on protein stability and folding by fluorescence-based thermal shift assays in the presence and absence of gap DNA (Supplementary Figure 5). In comparison with T_m of ~44 °C for wild-type polβ, we observed relatively lower thermal stability for SM, TM1, TM2, and DM/TM mutants and a slightly higher T_m value for DM mutant (Supplementary Figure 5A). There is an evident rightward shift in the thermal stability in the presence of gap DNA for polβ wild-type and all five mutats tested (Supplementary Figure 5B), suggesting that gap DNA has a stabilizing effect on polβ protein with and without the mutations that reside in DNA synthesis or dNTP selection subdomains of polβ.

Gap filling efficiency of polβ variants

To investigate the impact of the polβ mutations on BER activity of the enzyme, we performed gap filling assays for correct, mismatch, and oxidized nucleotide insertions *in vitro*. Our results showed no significant difference between wild-type polβ and all five variants tested in this study for dGTP:C insertion (Figure 7A and Supplementary Figure 6). Similar to wild-type enzyme, the polβ variants exhibit inefficient gap filling for the mismatch incorporations of dTTP and dCTP opposite C (Figure 7B,C and Supplementary Figures 7-8). However, for the dATP:C mismatch, our results showed an increase in the amount of gap filling products for the polβ mutants TM2 (L301R/V303R/V306R) and DM/TM (L301R/V303R/V306RK206A/K244A) (Figure 7D and Supplementary Figure 9). This could be due to a particular mismatch insertion preference of wild-type polβ as reported in the crystallographic pre-mutagenic structures of dC-dAMPCPP mismatch that forms a closed conformation at the active site, which is identical to the polβ structure with Watson-Crick base pair.[46] We also tested all possible template G mismatches, dATP:G, dTTP:G, and dGTP:C, and observed a higher amount of mismatch insertion products for polβ TM2 and DM/TM mutants particularly for dATP:G mismatch (Figure 8 and Supplementary Figure 10). We finally aimed to understand the impact of polβ/XRCC1 interaction mutants on the efficiency for mutagenic insertion of 8oxodGTP opposite A (Figure 9A). Our results demonstrated ~2-fold decrease in the efficiency of oxidized nucleotide insertion between polβ wild-type and cancer-associated T304I single mutant at earlier time points of the reaction (Figure 9B, lanes 2–5 *versus* 6–10). We obtained almost wild-type level of 8oxodGTP:A insertion for other polβ variants tested in this study (Figure 9C) and no significant difference in the amount of insertion products (Figure 9D). Overall results revealed the most significant impact on polβ gap filling activity with polβ TM2 and DM/TM mutants harboring mutations in the V303 loop region that is located in the dNTP selection subdomain of the protein.

Impact of polβ variants on the ligation of correct nucleotide insertion products by DNA ligase IIIα in the absence and presence of XRCC1

In addition to the nucleotide insertion assays, we investigated polβ variants to understand the efficiency of the substrate-product channeling process with DNA ligase at the downstream steps of the BER pathway. For this purpose, we used one nucleotide gap DNA substrate with a template C and performed coupled assays to measure polβ correct nucleotide insertion (dGTP:C) coupled to nick sealing at the same time points of incubation in the reaction mixture including the polβ (wild-type or mutants) and LIGIIIα (Figure 10A).

For the reaction mixture containing wild-type polβ and LIGIIIα (Figure 10B, lanes 2–5), we show the time course of ligation product formation after gap filling (*i.e.*, nick sealing of polβ dGTP:C insertion products). Similarly, for polβ variants T304I and DM carrying K206A/K244A mutations (Figure 10B, lanes 6–9 and 10–13, respectively) as well as the triple-mutants, T304I/K206A/K244A and L301R/V303R/V306R, we obtained the ligation products of polβ dGTP:C insertions (Figure 10C, lanes 2–5 and 6–9, respectively). For the polβ V303 loop region mutant DM/TM carrying L301R/V303R/V306RK206A/K244A mutations (Figure 10C, lanes 10–13), there was a slight difference in the amount of ligation products (Figure 10D) when compared to wild-type polβ. Overall, our results demonstrated that polβ variants can insert dGTP opposite template C in a gap DNA, and the resulting nick repair product can be ligated by LIGIIIα.

In addition, we performed the same coupled assays in the presence of XRCC1 to test the effect of the scaffolding factor on the ligation of dGTP:C insertion products by polβ wild-type *versus* variants (Figure 11A). With the addition of XRCC1 to the reaction mixture, including wild-type polβ and LIGIIIα, we obtained more ligation product along with simultaneous disappearance of the gap filling product (Figure 11B, lanes 2–5). Similarly, we observed efficient ligation of polβ dGTP:C insertion products in the presence of XRCC1 in the coupled reactions including polβ variants T304I (Figure 11B, lanes 6–9), DM (Figure 11B, lanes 10–13), and TM1 (Figure 11C, lanes 2–5). For those polβ variants, there was a relatively higher amount of ligation products at initial time points when compared to the ligation products in the absence of XRCC1 (Supplementary Figure 11). These results suggest that XRCC1 facilitates the conversion of polβ dGTP:C insertion products to the complete ligation products by LIGIIIα. However, for the polβ variants TM2 and DM/TM (Figure 11C, lanes 6–9 and 10–13, respectively), there was no effect of XRCC1 on the ligation of polβ dGTP:C insertion products by LIGIIIα, as we might predict since these mutants do not bind to XRCC1. We obtained almost the same amount of ligation products in the coupled reactions including polβ TM2 and DM/TM mutants in the absence and presence of XRCC1 (Supplementary Figure 11).

Impact of polβ variants on the ligation of oxidized nucleotide insertion products by DNA ligase IIIα

We previously demonstrated that polβ oxidized nucleotide insertion confounds the nick sealing step of BER, leading to a ligation failure and an interruption in the coordinated repair pathway.[41] To further understand the impact of polβ variants on the ligation efficiency at the downstream steps involving LIGIIIα activity, in addition to correct nucleotide insertion

assays, we questioned the ligation efficiency after oxidized nucleotide (8oxodGTP:A) insertions by polβ variants (Figure 12A). For this purpose, we only investigated polβ mutants SM (T304I) and TM2 (L301R/V303R/V306R).

In line with our previous findings,[41] for wild-type polβ, we found that polβ 8oxodGTP insertion leads to a failure in nick sealing by LIGIIIα and results in the formation of abortive ligation products with 5'-AMP (Figure 12B, lanes 2–5). For the polβ variants T304I and TM2, we also obtained both mutagenic nick sealing of polβ 8-oxodGTP insertion product and ligation failure (Figure 12B, lanes 6–9 and 10–13, respectively). However, for those polβ variants, we observed relatively less mutagenic ligation and more failure products when compared with wild-type polβ (Figure 12C,D).

Discussion

BER, an essential repair mechanism that maintains nuclear and mitochondrial genome stability, is responsible for the repair of single DNA base lesions as well as single-strand breaks that can be formed during endogenous cellular processes or by the effects of multiple exogenous factors.[1–6] Dysfunctional BER has been linked to many human maladies such as neurodegenerative diseases and cancer, and many such aberrations have been associated with the mutations in the genes for BER proteins, residing in the regions that mediate protein–protein interactions or that impact expression levels.[47–49] The BER pathway involves several core proteins working in a sequential manner by the mechanism known as substrate-product channeling to transfer DNA intermediates from one enzyme to the next in the pathway.[11–18] This mechanism promotes the efficiency of BER and minimizes the release of potentially toxic repair intermediates into the cell. Although the roles of individual BER enzymes have been established at biochemical and structural levels greatly, it is still unknown how BER proteins function as a multi-protein complex to enable efficient repair. Protein-protein interactions are what make the assembly and function of the repair complexes possible, thus mutations in the core BER proteins can compromise the formation of the repair protein complexes and efficiency of DNA damage processing.[50,51]

Polβ is the primary BER polymerase and performs critical functions, dRP-group removal and DNA synthesis, which creates a nick repair product that can be handed over to the next enzyme, LIGI or LIGIIIα, at the downstream steps of BER pathway.[52] Studies have found that a large portion of human cancers have mutations in the polβ gene, for example, ~ 75% of the tumors analyzed in a colon cancer cohort were found to carry mutations in the coding region of the polβ gene.[53] These variants have been shown to induce chromosomal aberrations, exhibit cellular transformation when expressed in both human and mouse cells, and untimately lead to genomic instability.[54] XRCC1, a non-enzymatic scaffolding protein, is thought to promote repair protein recruitment to the site of DNA damage and facilitates the substrate-product channeling process between the core components of BER pathway via the protein–protein interactions with downstream factors so that the release and accumulation of toxic intermediates can be avoided.[21,22] Thus, it is important to investigate the role of the key repair factors that maintain BER accuracy, particularly XRCC1, and how mutations at the interaction interfaces of multi-protein BER complexes scaffolded by XRCC1 could affect the efficiency of the repair pathway coordination.

Although XRCC1 tightly interacts with polβ as revealed by the structure of the polβ/XRCC1 heterodimer repair complex comprised of the carboxy-terminal domain of polβ and the amino-terminal domain of human XRCC1,[30–32] mouse models and cellular studies with XRCC1-deficient mouse fibroblasts demonstrated polβ-dependent cell survival independent of XRCC1 expression in response to DNA methylating agent methyl methanesulfonate and PARP inhibitors.[34–37,55–58] Interestingly, mutation of the mouse polβ gene that blocks the interaction with XRCC1, yields a viable mouse, albeit smaller in staure.[59] LIGIIIα forms a stable complex with XRCC1 through BRCT domains of both proteins and reduced steady-state levels of both polβ and LIGIIIα have been shown in XRCC1-deficient cells, indicating that XRCC1 interactions promote the stability of these DNA repair enzymes along with their recruitment to DNA damage sites.[60] However, the mechanism by which XRCC1 regulates the repair pathway coordination at the downstream steps involving polβ and LIGIIIα activities is not fully understood.

Previous studies have shown that the cellular homeostasis and stability of polβ and XRCC1 are crucial for their cellular functions and to maintain genomic stability.[39,40] It has been shown that once released from XRCC1, polβ is ubiquitylated on the lysine residues K206/K244 that are located at the C-terminal domain of the protein and degraded by the proteasome independent pathway. Polβ/XRCC1 interaction mutants exhibit higher levels of proteosome mediated degradation and XRCC1 helps to protect polβ from ubiquitin-dependent degradation pathways, but that polβ colon cancer-associated variant T304I was still unstable even after mutating residues that are targeted for ubiquitylation (K206A/K244A). Furthermore, XRCC1 that is not bound to polβ forms a complex with HSP90 that stabilizes XRCC1 protein levels and the cells expressing polβ-XRCC1 interaction mutants exhibit an increase in presence of XRCC1/HSP90 heterodimer.[39,40] Although the biological importance of XRCC1's scaffolding function in the context of genomic stress through its interactions with polβ has been extensively studied, the mechanistic understanding of the BER pathway coordination by the downstream proteins (polβ/XRCC1/LIGIIIα/gap DNA) scaffolded by XRCC1 and how the aberrations in this coordination through the mutations that affect protein interactome and cellular stability of individual components of the BER multi-protein complex remains largely unknown.

In this study, we investigated the polβ variants T304I (SM), K206A/K244A (DM), T304I/K206A/K244A (TM1), L301R/V303R/V306R (TM2), and K206A/K244A/L301R/V303R/V306R (DM/TM) carrying the mutations that reside either in the V303 loop, the interface of protein interaction with XRCC1 or at the lysine residues, K206 and K244, that are critical for polβ ubiquitylation and stability. Our findings demonstrated lack of a stable protein complex formation and interaction with XRCC1 in the presence of the mutations in the V303 loop alone (TM2) and in combination with the mutated ubiquitylation sites (DM/TM). Although the mutations did not affect the gap DNA binding affinity of the wild-type enzyme, we demonstrated an increased mismatch insertion efficiency with these polβ variants and difference in the mutagenic insertion of 8oxodGTP:A. It has been reported in many studies that the fidelity of BER is dependent on the DNA synthesis step of the repair pathway, where polβ selects and inserts the correct Watson-Crick base paired nucleotide into a gap repair intermediate. Therefore, polβ variants with aberrant BER function can affect the efficiency of the repair pathway coordination, which could lead to a mutator phenotype or

genomic instability as shown in 30% of human tumors carrying mutations in polβ gene and are associated with many types of cancers.[38,54]

Moreover, although none of the mutants showed a significantly altered binding affinity to nick DNA compared to wild-type polβ, our results demonstrated an enhanced ligation of the nick repair intermediate after dGTP:C nucleotide insertion by polβ colon cancer-associated variant T304I as well as SM and TM1 mutants in the presence of XRCC1, suggesting that the scaffolding factor could promote efficient hand-off of the nick repair product to LIGIIIα for nick sealing in the downstream steps of BER pathway. However, this substrate-product channeling process is compromised by combined mutations that are located in both V303 loop and the ubiquitylation region of polβ. Similarly, LIGIIIα fails in nick sealing of oxidized nucleotide 8oxodGTP:A insertion products by polβ variants TM2 and DM/TM resulting in the formation of ligation failure products that are relatively higher than polβ wild-type. Overall, our findings provide mechanistic insight into how the multi-protein complex, particularly the downstream proteins polβ/LIGIIIα/XRCC1, could govern efficient hand off process during BER and the mutations in the critical interaction interfaces may lead to inaccurate repair coordination at the last steps involving gap filling by polβ coupled to nick sealing by LIGIIIα in the presence and absence of XRCC1 interactions.

LIG1 and LIGIIIα finalize BER by sealing DNA ends of nick repair product at the last ligation step. Both BER ligases are exchangeable and support robust ligation activity in reconstituted repair assays *in vitro*.[3] Interestingly, LIG1 appears to be more critical ligase in the repair of nuclear DNA damage induced by methyl methanesulfonate.[61] Furthermore, it has been reported that LIG1 is a predictor of platinum resistance and its blockade is synthetically lethal in XRCC1 deficient epithelial ovarian cancers.[62] In addition to LIGIIIα as we studied in the present work, future studies are required to investigate the role of LIGI for the functional interplay with polβ variants, and how the mutations could affect the repair pathway coordination through polβ/XRCC1 interaction at the downsteam steps involving LIG1 acitivity.

Because the amino acid substitutions of the polβ variants examined in this study are located in the polymerase domain, particularly in the dNTP selection (262–335 aa) and DNA synthesis (149–262 aa) subdomains of the polβ protein (Figure 1), they might represent separation-of-function mutants that are deficient either in one or a number of interactions. Therefore, further protein–protein interaction studies with other core repair enzymes that function at earlier steps of the repair pathway, such as DNA glycosylases (OGG1, UDG) and APE1, are required to comprehensively investigate the impact of these polβ variants on the BER pathway coordination. As the current models suggest that polβ/XRCC1 function as a static heterodimeric complex at sites of DNA repair, which is critical for XRCC1-mediated recruitment of polβ to foci of DNA damage and repair, future structure/function studies of the polβ variants alone and in complex with NTD region of XRCC1 at atomic resolution as well as a large BER protein assemblies of polβ/XRCC1/LIGIIIα complexes through cryo-EM can help to map the impact of the mutations on the interaction interface and to better understand how XRCC1 could serve as a platform to recruit the repair complex in case of the polβ mutations affecting its repair function and/or interactions.

Defining the molecular determinants that dictate BER accuracy, particularly in the context of pathway coordination, is critical to fully understand disease mechanisms. Elucidating the interface of BER interactome within large protein assemblies of the repair complexes is of high importance for exploiting as novel targets for future rational chemotherapeutic drug design toward enhancing human health.[63–65] Furthermore, the somatic mutations in critical protein–protein interaction interfaces of BER complexes could alter the enzyme function and sub-cellular localization of the repair protein, and therefore interfere with the pathway coordination and efficiency of BER, which in turn can regulate cellular response to genotoxic stress. Therefore, providing mechanistic insights into the molecular elements that govern the repair pathway coordination, and defining the cellular consequences of defective BER could be considered as a therepautic target to advise disease risk assessments and potentially identify BER coordination-specific mutational patterns.

Supplementary Material

Refer to Web version on PubMed Central for supplementary material.

Acknowledgements

We thank Dr. Robert McKenna (University of Florida) for his support regarding the Biacore X100 (Cytiva) to perform SPR assays. The authors thank the Monoclonal Antibody Core at the ICBR (University of Florida) and Dr. Angel Samson for her assistance regarding the Octet Qke (Fortebio) to perform the biolayer interferometry assays. R.W.S is the Dean’s Professor of Cancer Research in the Department of Pathology and Laboratory Medicine at the Warren Alpert Medical School, Brown University.

Funding

This work was supported by a grant 1R35GM147111-01 from the National Institute of General Medical Sciences (NIGMS). Research in the Sobol lab on DNA repair, the analysis of DNA damage, and the impact of genotoxic exposure is funded by grants from the NIH [ES029518, ES028949, CA238061, CA236911, AG069740, and ES032522], and from the NSF [NSF-1841811]. Support is also provided by the Legoretta Cancer Center Endowment Fund (to R. W.S.).

Data Availability

All data are contained within the article. Further information and requests of materials used in this research should be directed to Melike Çaglayan (caglayanm@ufl.edu).

References

1. Krokan HE et al. , (2000). Base excision repair of DNA in mammalian cells. FEBS Letter 476, 73–77.
2. Lindahl T, (2001). Keynote: past, present, and future aspects of base excision repair. Prog. Nucleic Acid Res. Mol. Biol. 68, xvii–xxx. [PubMed: 11554316]
3. Beard WA et al. , (2019). Eukaryotic base excision repair: new approaches shine light on mechanism. Ann. Rev. Biochem. 88, 137–162. [PubMed: 31220977]
4. Parikh SS, Mol CD, Tainer JA, (1997). Base excision repair enzyme family portrait: integrating the structure and chemistry of an entire DNA repair pathway. Structure 5, 1543–1550. [PubMed: 9438868]
5. Hitomi K, Iwai A, Tainer JA, (2007). The intricate structural chemistry of base excision repair machinery: implications for DNA damage recognition, removal, and repair. DNA Repair 6, 410–428. [PubMed: 17208522]

6. Kim YJ, Wilson DM, (2012). Overview of base excision repair biochemistry. Curr. Mol. Pharmacol. 5, 3–13. [PubMed: 22122461]
7. Almeida KH, Sobol RW, (2012). A unified view of base excision repair: lesion-dependent protein complexes regulated by post-translational modification. DNA Repair 6, 695–711.
8. Fortini P, Parlanti E, Sidorkina OM, Laval J, Dogliotti E, (1999). Type of DNA glycosylase determines the base excision repair pathway in mammalian cells. J. Biol. Chem. 274, 15230–15236. [PubMed: 10329732]
9. Beard WA, Prasad R, Wilson SH, (2006). Activities and mechanism of DNA polymerase β. Methods Enzymol. 408, 91–107. [PubMed: 16793365]
10. Tomkinson AE, Vijayakumar S, Pascal JM, Ellenberger T, (2006). DNA ligases: structure, reaction mechanism, and function. Chem. Rev. 106, 687–699. [PubMed: 16464020]
11. Wilson SH, Kunkel TA, (2000). Passing the baton in base excision repair. Nature Struct. Biol. 7, 176–178. [PubMed: 10700268]
12. Prasad R, Shock DD, Beard WA, Wilson SH, (2010). Substrate channeling in mammalian base excision repair pathways: passing the baton. J. Biol. Chem. 285, 40479–40488. [PubMed: 20952393]
13. Prasad R et al. , (2011). A review of recent experiments on step-to-step "hand-off" of the DNA intermediates in mammalian base excision repair pathways. Mol. Biol. 45, 586–600.
14. Saville KM et al. , (2020). NAD^+-mediated regulation of mammalian base excision repair. DNA Repair 93, 102930 [PubMed: 33087267]
15. Srivastava DK et al. , (1998). Mammalian abasic site base excision repair. Identification of the reaction sequence and rate-determining steps. J. Biol. Chem. 273, 21203–21209. [PubMed: 9694877]
16. Moor NA et al. , (2015). Quantitative characterization of protein-protein complexes involved in base excision DNA repair. Nucleic Acids Res. 43, 6009–6022. [PubMed: 26013813]
17. Liu Y et al. , (2007). Coordination of steps in single-nucleotide base excision repair mediated by apurinic/apyrimidinic endonuclease 1 and DNA polymerase beta. J. Biol. Chem. 282, 13532–13541. [PubMed: 17355977]
18. Prasad R, Williams JG, Hou EW, Wilson SH, (2012). Pol β associated complex and base excision repair factors in mouse fibroblasts. Nucleic Acids Res. 40, 11571–11582. [PubMed: 23042675]
19. Caglayan M, Wilson SH, (2015). Oxidant and environmental toxicant-induced effects compromise DNA ligation during base excision DNA repair. DNA Repair 35, 85–89. [PubMed: 26466358]
20. Caglayan M, (2019). Interplay between DNA polymerases and DNA ligases: Influence on substrate channeling and the fidelity of DNA ligation. J. Mol. Biol. 431, 2068–2081. [PubMed: 31034893]
21. Caldecott KW, (2003). XRCC1 and DNA strand break repair. DNA Repair 2, 955–969. [PubMed: 12967653]
22. Caldecott KW, (2019). XRCC1: Protein, form, and function. DNA Repair 81, 102664 [PubMed: 31324530]
23. Beernink PT et al. , (2005). Specificity of protein interactions mediated by BRCT domains of the XRCC1 DNA repair protein. J. Biol. Chem. 280, 30206–30213. [PubMed: 15987676]
24. Vidal AE et al. , (2001). XRCC1 coordinates the initial and late stages of DNA abasic site repair through protein-protein interactions. EMBO J. 20, 6530–6539. [PubMed: 11707423]
25. Campalans A et al. , (2005). XRCC1 interactions with multiple DNA glycosylases: a model for its recruitment to base excision repair. DNA Repair 4, 826–835. [PubMed: 15927541]
26. Marsin S et al. , (2003). Role of XRCC1 in the coordination and stimulation of oxidative DNA damage repair initiated by the DNA glycosylase hOGG1. J. Biol. Chem. 278, 44068–44074. [PubMed: 12933815]
27. Akbari M et al. , (2010). Direct interaction between XRCC1 and UNG2 facilitates rapid repair of uracil in DNA by XRCC1 complexes. DNA Repair 9, 785–795. [PubMed: 20466601]
28. Caldecott KW et al. , (1996). XRCC1 polypeptide interacts with DNA polymerase β and possibly poly(ADP-ribose) polymerase, and DNA ligase III is a novel molecular 'nick-sensor' in vitro. Nucleic Acids Res. 24, 4387–4394. [PubMed: 8948628]

29. Cappelli E et al. , (1997). Involvement of XRCC1 and DNA ligase III gene products in DNA base excision repair. J. Biol. Chem. 272, 23970–23975. [PubMed: 9295348]
30. Marintchev A et al. , (2000). Domain specific interaction in the XRCC1-DNA polymerase β complex. Nucleic Acids Res. 28, 2049–2059. [PubMed: 10773072]
31. Gryk MR et al. , (2002). Mapping of the interaction interface of DNA polymerase β with XRCC1. Structure 10, 1709–1720. [PubMed: 12467578]
32. Marintchev A, Gryk MR, Mullen GP, (2003). Site-directed mutagenesis analysis of the structural interaction of the single-strand-break protein, X-ray cross-complementing group 1, with DNA polymerase β. Nucleic Acids Res. 31, 580–588. [PubMed: 12527765]
33. Tang Q, Caglayan M, (2021). The scaffold protein XRCC1 stabilizes the formation of polβ/gap DNA and ligase IIIα/nick DNA complexes in base excision repair. J. Biol. Chem. 297, 101025 [PubMed: 34339737]
34. Brem R, Hall J, (2005). XRCC1 is required for DNA single-strand break repair in human cells. Nucleic Acids Res. 33, 2512–2520. [PubMed: 15867196]
35. Dianova II et al. , (2004). XRCC1-DNA polymerase β interaction is required for efficient base excision repair. Nucleic Acids Res. 32, 2550–2555. [PubMed: 15141024]
36. Horton JK et al. , (2008). XRCC1 and DNA polymerase b in cellular protection against cytotoxic DNA single-strand breaks. Cell Res. 18, 48–63. [PubMed: 18166976]
37. Wong HK, Wilson DM, (2005). XRCC1 and DNA polymerase β interaction contributes to cellular alkylating-agent resistance and single-strand break. J. Cell. Biochem. 95, 794–804. [PubMed: 15838887]
38. Donigan KA et al. , (2012). Human POLB gene is mutated in high percentage of colorectal tumors. J. Biol. Chem. 287, 23830–23839. [PubMed: 22577134]
39. Fang Q et al. , (2014). HSP90 regulates DNA repair via the interaction between XRCC1 and DNA polymerase β. Nature Commun. 5, 5513. [PubMed: 25423885]
40. Fang Q et al. , (2019). Stability and sub-cellular localization of DNA polymerase β is regulated by interactions with NQO1 and XRCC1 in response to oxidative stress. Nucleic Acids Res. 47, 6269–6286. [PubMed: 31287140]
41. Çağlayan M et al. , (2017). Oxidized nucleotide insertion by pol β confounds ligation during base excision repair. Nature Commun. 8, 14045. [PubMed: 28067232]
42. Çağlayan M, (2020). The ligation of pol β mismatch insertion products governs the formation of promutagenic base excision DNA repair intermediates. Nucleic Acids Res. 48, 3708–3721. [PubMed: 32140717]
43. Çağlayan M, (2020). Pol β gap filling, DNA ligation and substrate-product channeling during base excision repair opposite oxidized 5-methylcytosine modifications. DNA Repair 95, 102945 [PubMed: 32853828]
44. Tang Q, Kamble P, Çağlayan M, (2020). DNA ligase I variants fail in the ligation of mutagenic repair intermediates with mismatches and oxidative DNA damage. Mutagenesis 35, 391–404. [PubMed: 32914844]
45. Kamble P, Hall K, Chandak M, Tang Q, Çağlayan M, (2021). DNA ligase I fidelity the mutagenic ligation of pol β oxidized and mismatch nucleotide insertion products in base excision repair. J. Biol. Chem. 296, 100427 [PubMed: 33600799]
46. Batra VK et al. , (2008). Structures of DNA polymerase β with active site mismatches suggest a transient abasic site intermediate during misincorporation. Mol. Cell 30, 315–324. [PubMed: 18471977]
47. Karahalil B, Bohr VA, Wilson DM, (2012). Impact of DNA polymorphisms in key DNA base excision repair proteins on cancer risk. Hum. Exp. Toxicol. 31, 981–1005. [PubMed: 23023028]
48. Wallace SS, Murphy DL, Sweasy JB, (2012). Base excision repair and cancer. Cancer Letter 327, 73–89.
49. Ramakodi MP et al. , (2017). Integrative genomic analysis identifies ancestry-related expression quantitative trait loci on DNA polymerase β and supports the association of genetic ancestry with survival disparities in head and neck squamous cell carcinoma. Cancer 123, 849–860. [PubMed: 27906459]

50. Abbotts R, Wilson DM, (2017). Coordination and DNA single strand break repair. Free Radic. Biol. Med. 107, 228–244. [PubMed: 27890643]
51. Moor NA, Lavrik OI, (2018). Protein-protein interactions in DNA base excision repair. Biochemistry 83, 411–422. [PubMed: 29626928]
52. Çağlayan M, (2019). Interplay between DNA polymerases and DNA ligases: Influence on substrate channeling and the fidelity of DNA ligation. J. Mol. Biol. 431, 2068–2081. [PubMed: 31034893]
53. Wallace SS, Murphy DL, Sweasy JB, (2012). Base excision repair and cancer. Cancer Letter 327, 73–89.
54. Sweasy JB et al. , (2005). Expression of DNA polymerase β cancer-associated variants in mouse cells results in cellular transformation. Proc. Natl. Acad. Sci. U S A 102, 14350–14355. [PubMed: 16179390]
55. Horton JK et al. , (2000). Protection against methylation-induced cytotoxicity by DNA polymerase β-dependent base excision repair. J. Biol. Chem. 275, 2211–2218. [PubMed: 10636928]
56. Horton JK et al. , (2003). Hypersensitivity of DNA polymerase β null mouse fibroblasts reflects accumulation of cytotoxic repair intermediates from site-specific alkyl DNA lesions. DNA Repair 2, 27–48. [PubMed: 12509266]
57. Horton JK et al. , (2013). Preventing oxidation of cellular XRCC1 affects PARP-mediated DNA damage responses. DNA Repair 12, 774–785. [PubMed: 23871146]
58. Horton JK et al. , (2015). DNA polymerase β-dependent cell survival independent of XRCC1 expression. DNA Repair 26, 23–29. [PubMed: 25541391]
59. Koczor CQ et al. , (2023). polβ/XRCC1 heterodimerization dictates DNA damage recognition and basal polβ protein levels without interfering with mouse viability or fertility. DNA Repair 123, 103452 [PubMed: 36702010]
60. Caldecott KW et al. , (1994). An interaction between the mammalian DNA repair protein XRCC1 and DNA ligase III. Mol. Cell Biol. 14, 68–76. [PubMed: 8264637]
61. Gao Y et al. , (2011). DNA ligase III is critical for mtDNA integrity but not XRCC1-mediated nuclear DNA repair. Nature 471, 240–244. [PubMed: 21390131]
62. Ali R et al. , (2021). Ligase 1 is a predictor of platinum resistance and its blockade is synthetically lethal in XRCC1 deficient epithelial ovarian cancers. Theranostics 11, 8350–8361. [PubMed: 34373746]
63. Kelley MR, Logsdon D, Fishel ML, (2014). Targeting DNA repair pathways for cancer treatment: what's new? Future Oncol. 10, 1215–1237. [PubMed: 24947262]
64. Jubb H et al. , (2012). Structural biology and drug discovery for protein-protein interactions. Trends Pharmacol Sci. 33, 241–248. [PubMed: 22503442]
65. Ivanov AA et al. , (2013). Targeting protein-protein interactions as an anticancer strategy. Trends Pharmacol. Sci. 34, 393–400. [PubMed: 23725674]

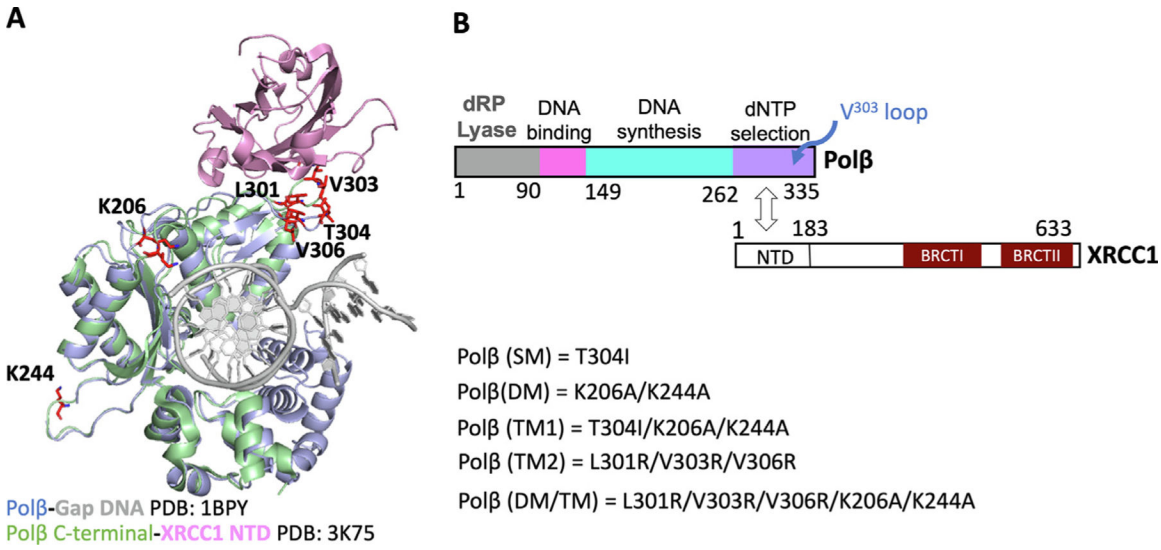

Figure 1. Structure model and protein domain organization of polβ variants.

(A) Ribbon representation illustrates polβ (blue) C-terminal domain (green) in interaction with XRCC1 N-terminal domain (pink) bound to gap DNA (grey). Polβ amino acid residues carrying the mutations that were examined in this study are K206, K244, L301, V303, T304, and V306, which are all represented in red. **(B)** XRCC1 interacts with polβ through its N-terminal domain (NTD), and a string of nine amino acids, namely the V303 loop, is the XRCC1 interaction interface on polβ. Polβ variants examined in this study are T304I (SM), K206A/K244A (DM), T304I/K206A/K244A (TM1), L301R/V303R/V306R (TM2), and L301R/V303R/V306RK206A/K244A (DM/TM) reside in DNA synthesis and dNTP selection subdomains of polβ protein.

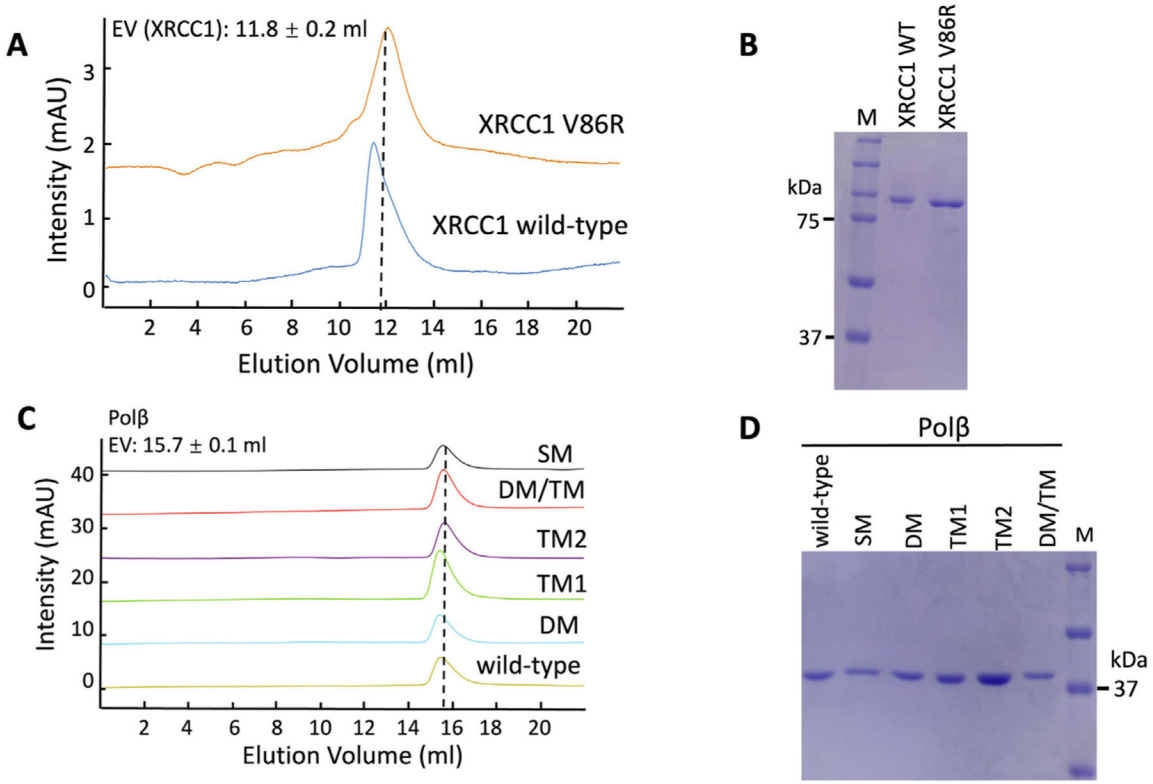

Figure 2. Size Exclusion Chromatography analyses of XRCC1 and polβ variants.

(A-B) The profiles of the elution volumes (EV) were presented for individual proteins XRCC1 wild-type and polβ/XRCC1 interaction-deficienct mutant V86R as 11.8 ml. **(C-D)** EV profiles were presented for individual proteins polβ wild-type and variants as 15.7 ml. Each peak fraction was analyzed on 12% SDS-polyacrylamide (w/v) gel and compared with the molecular weight marker. M represents a Precision Plus Protein Dual Color Standards (10–250 kDa).

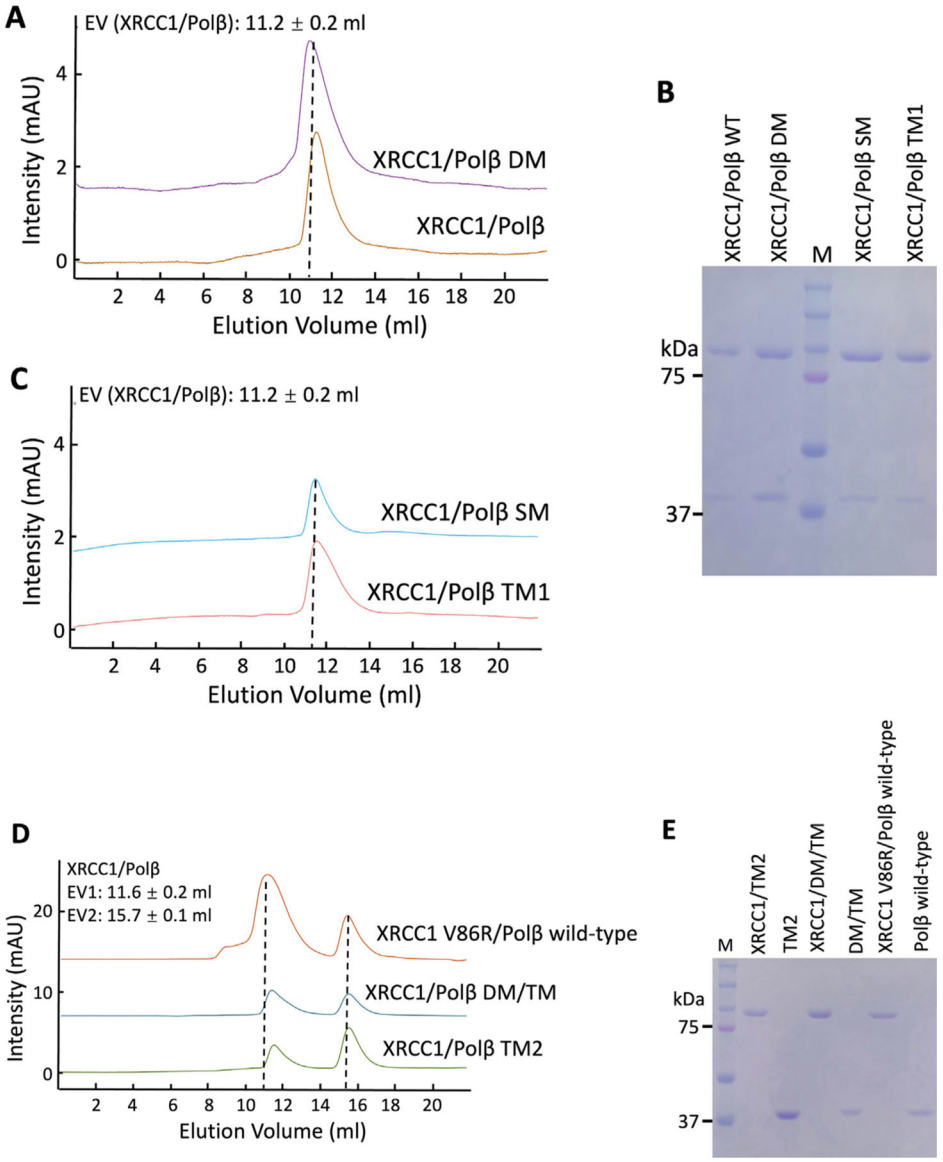

Figure 3. BER protein complex formation of XRCC1 and polβ variants.

The repair protein complexes were analyzed by SEC between XRCC1 and polβ wild-type or variants. **(A-C)** EV profiles are presented for a protein complex of XRCC1 and polβ wild-type or mutants SM, DM or TM1. **(D-E)** EV profiles are presented for a protein complex of XRCC1 mutant V866 and polβ wild-type as well as XRCC1 wild-type and polβ mutants TM2 or DM/TM. Each peak fraction is analyzed on 12% SDS-polyacrylamide (w/v) gel and compared with the molecular weight marker. M represents a Precision Plus Protein Dual Color Standard (10–250 kDa).

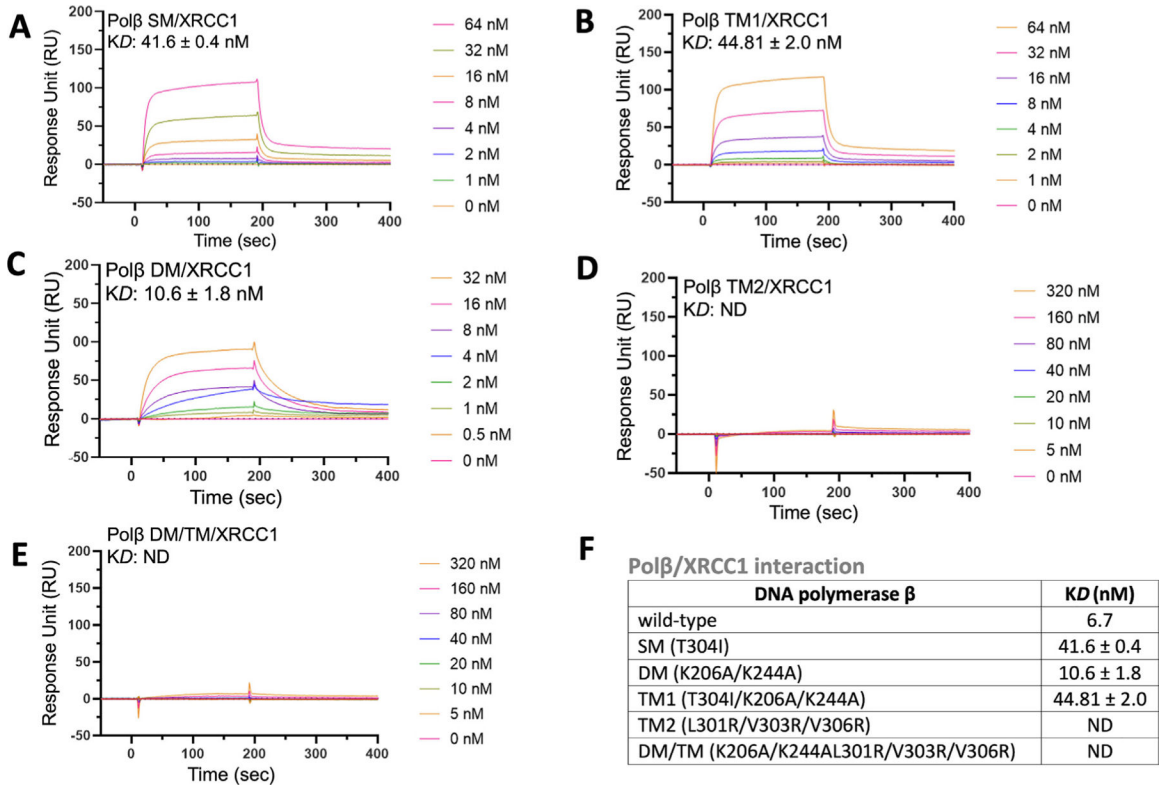

F

Polβ/XRCC1 interaction

DNA polymerase β	KD (nM)
wild-type	6.7
SM (T304I)	41.6 ± 0.4
DM (K206A/K244A)	10.6 ± 1.8
TM1 (T304I/K206A/K244A)	44.81 ± 2.0
TM2 (L301R/V303R/V306R)	ND
DM/TM (K206A/K244AL301R/V303R/V306R)	ND

Figure 4. Protein-protein interaction kinetics betwen polβ variants and XRCC1.

(A-E) Protein interaction kinetics are shown between XRCC1 and polβ mutants SM (A), TM1 (B), DM (C), TM2 (D), and DM/TM (E). **(F)** Table shows comparison of the equilibrium binding constants (K_D) between polβ wild-type and variants. Real-time interaction analyses were performed by surface plasmon resonance assay where GST-tag polβ was immobilized on CM5 biosensors. The ligand association and dissociation phases are shown for the protein concentration range of XRCC1 on the side of sensorgrams.

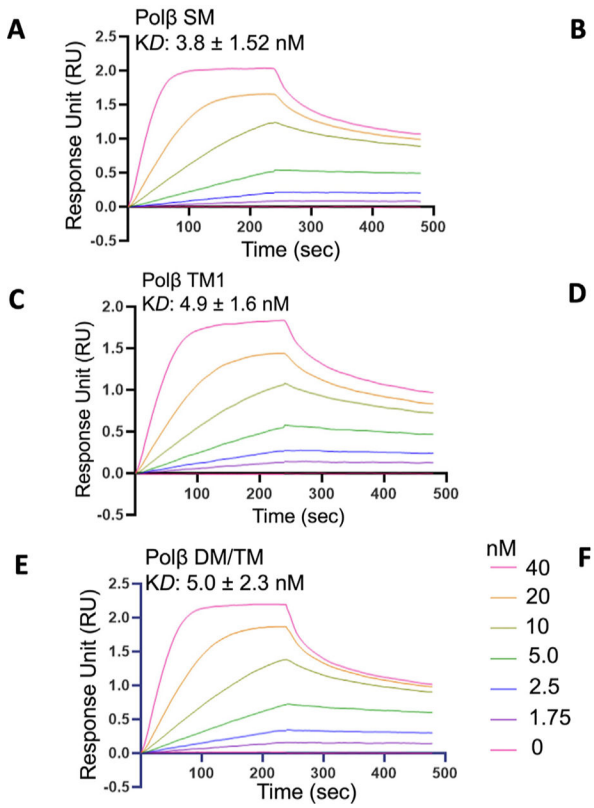

F

Gap DNA binding

DNA polymerase β	KD (nM)
wild-type	4.60 ± 1.90
SM (T304I)	3.80 ± 1.52
DM (K206A/K244A)	3.90 ± 1.20
TM1 (T304I/K206A/K244A)	4.90 ± 1.60
TM2 (L301R/V303R/V306R)	3.50 ± 1.50
DM/TM (K206A/K244AL301R/V303R/V306R)	5.0 ± 2.4

Figure 5. Gap DNA binding affinity of polβ variants.

(A-E) Real-time binding kinetics of one nucleotide gap DNA are shown for polβ mutants SM (A), DM (B), TM1 (C), TM2 (D), and DM/TM (E). The sensorgrams are shown for the concentrations range of polβ where gap DNA with a biotin label is immobilized on the streptavidin biosensors. **(F)** Table shows comparison of the equilibrium binding constants (K_D) between polβ wild-type and variants.

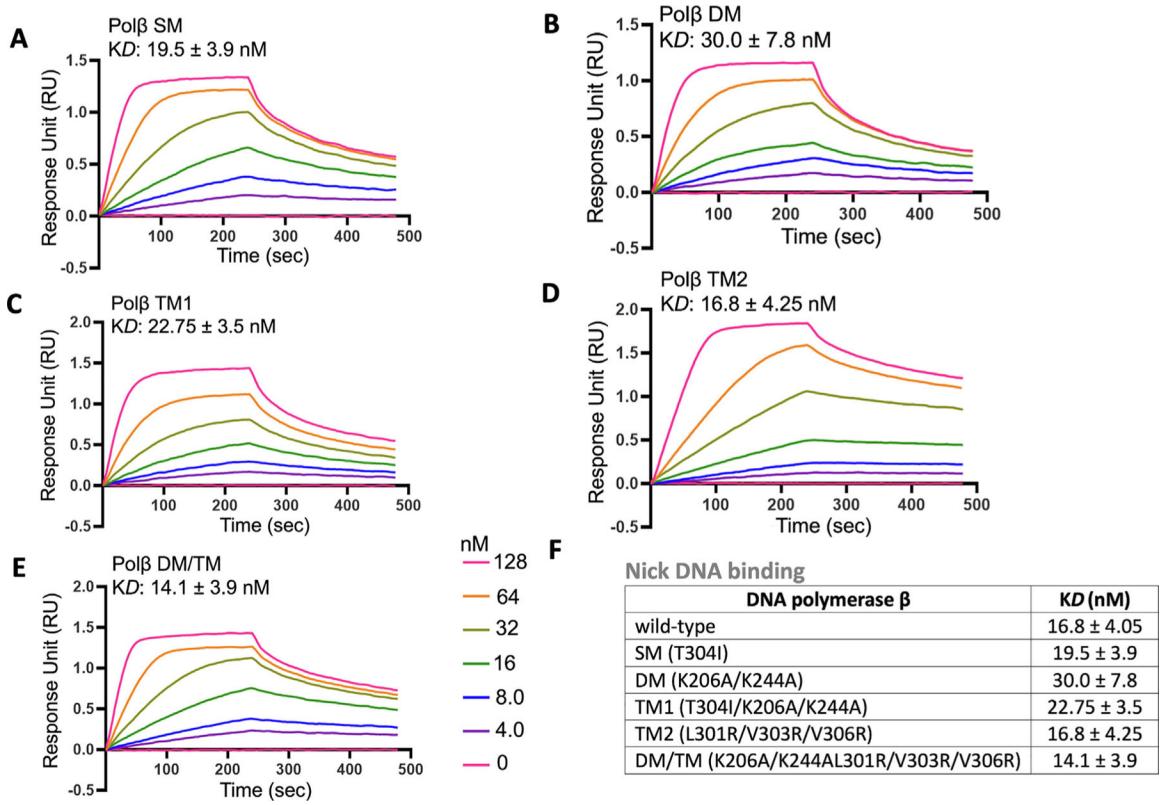

F

Nick DNA binding

DNA polymerase β	KD (nM)
wild-type	16.8 ± 4.05
SM (T304I)	19.5 ± 3.9
DM (K206A/K244A)	30.0 ± 7.8
TM1 (T304I/K206A/K244A)	22.75 ± 3.5
TM2 (L301R/V303R/V306R)	16.8 ± 4.25
DM/TM (K206A/K244AL301R/V303R/V306R)	14.1 ± 3.9

Figure 6. Nick DNA binding affinity of polβ variants.

(A-E) Real-time binding kinetics of nick DNA are shown for polβ mutants SM (A), DM (B), TM1 (C), TM2 (D), and DM/TM (E). The sensorgrams are shown for the concentrations range of polβ where nick DNA with a biotin label is immobilized on the streptavidin biosensors. **(F)** Table shows comparison of the equilibrium binding constants (K_D) between polβ wild-type and variants.

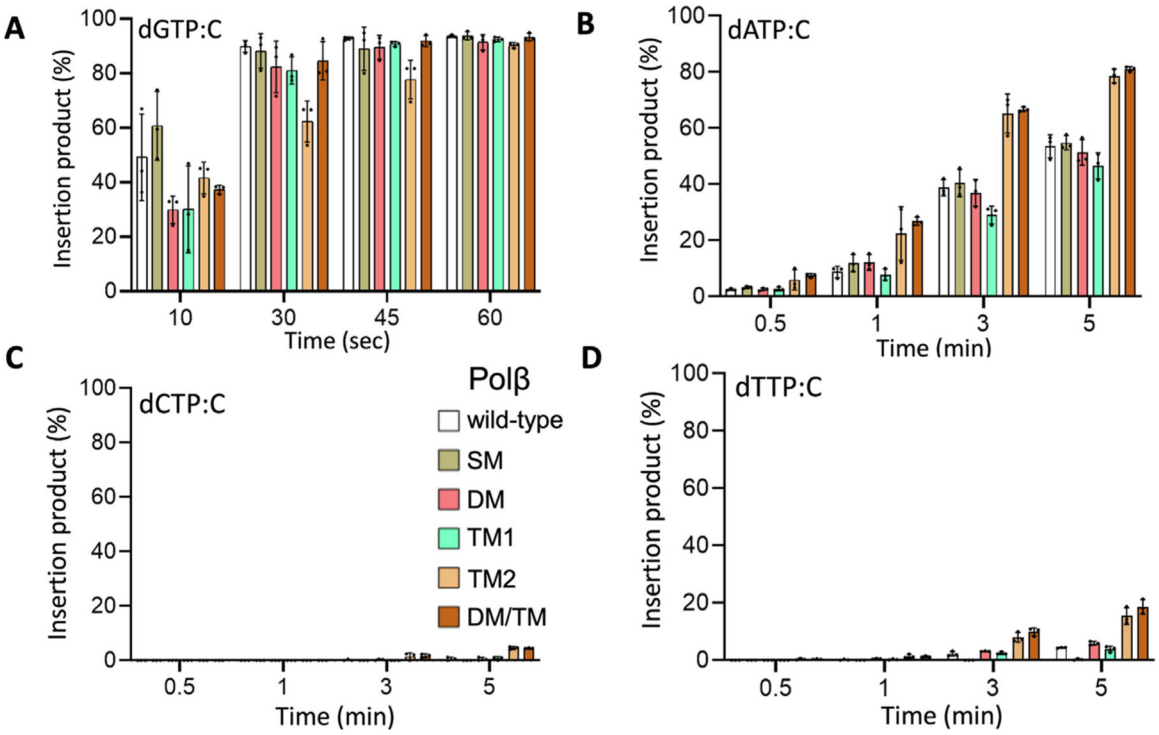

Figure 7.

Impact of polβ mutations on correct and mismatch insertion efficiency. (A-D) Graphs show time-dependent change in the amount of nucleotide insertion products for correct dGTP:C (A), mismatches dATP:C (B), dCTP:C (C), dTTP:C (D). The data represent the average of three independent experiments ± SD. The gel images showing polβ insertion substrate and products are presented in Supplementary Figures 6-9.

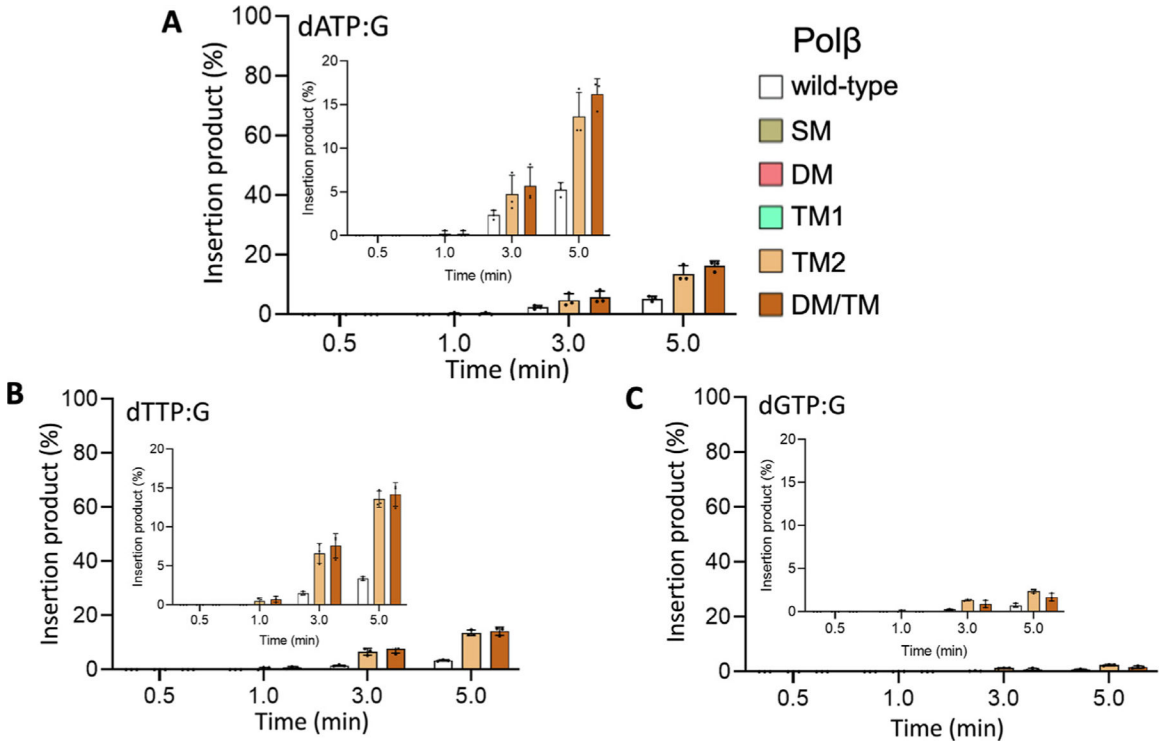

Figure 8.

Impact of polβ mutations on mismatch insertions. (A-C) Graphs show time-dependent change in the amount of mismatch insertion products for dATP:G (A), dTTP:G (B), dGTP:G (C). The data represent the average of three independent experiments ± SD. The gel images showing polβ insertion substrate and products are presented in Supplementary Figure 10.

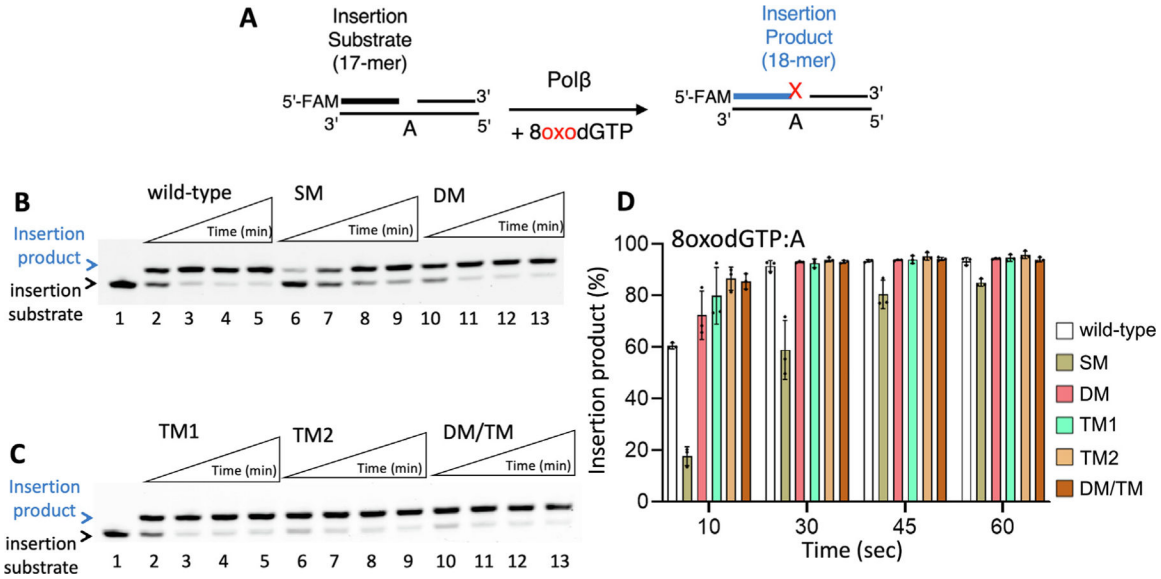

Figure 9. Efficiency of oxidized nucleotide insertion by polβ variants.

(A) Illustration of one nucleotide gap DNA substrate and insertion product in the insertion assay including polβ and 8oxodGTP. **(B-C)** Line 1 is the negative enzyme control of the one nucleotide gap DNA substrate. Lanes 2–5, 6–9 and 10–13 are 8oxodGTP:A insertion products by polβ wild-type, T304I, and DM mutants, respectively (B), and polβ TM1, TM2, and DM/TM mutants, respectively (C), and correspond to time points of 10, 30, 45, and 60 s. **(D)** Graph shows time-dependent change in the amount of nucleotide insertion and the data represent the average of three independent experiments ± SD.

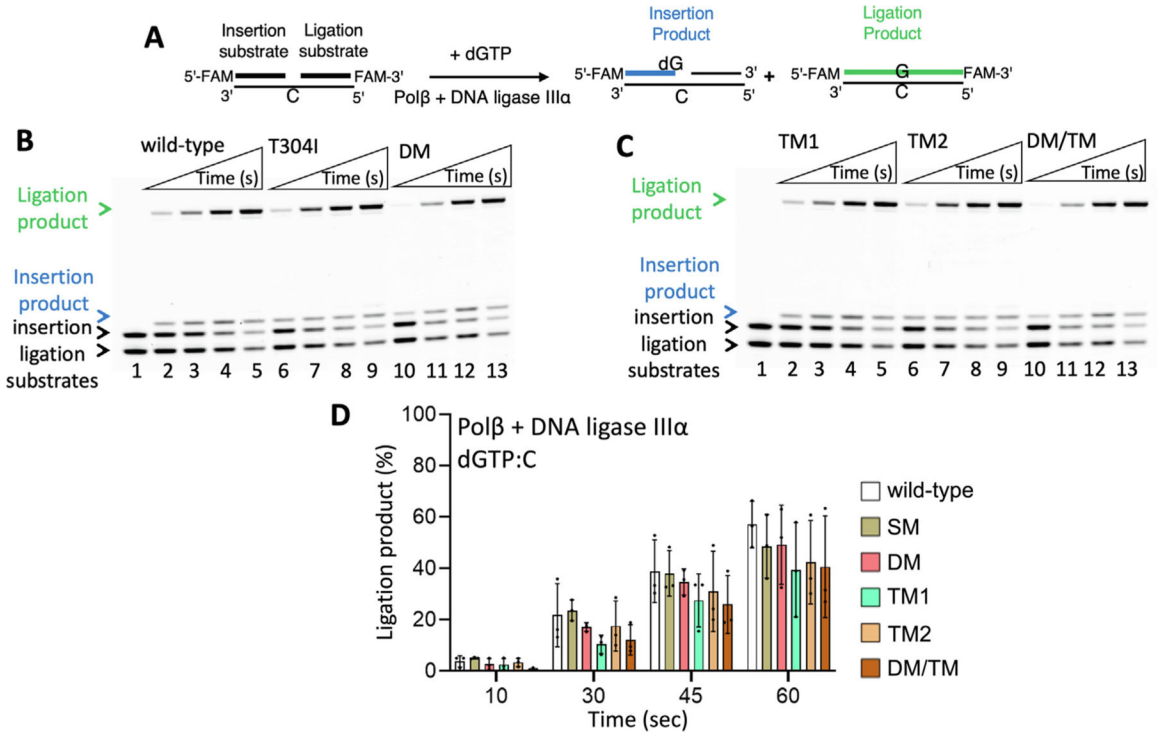

Figure 10. Impact of polβ mutations on the ligation of nucleotide insertion products by DNA ligase IIIα.

(A) Illustration of one nucleotide gap DNA substrate and the products of insertion and ligation in the coupled assays including polβ, LIGIIIα, and dGTP. **(B)** Line 1 is the negative enzyme control of the one nucleotide gap DNA substrate. Lanes 2–5, 6–9 and 10–13 are the ligation of dGTP:C insertion products by LIGIIIα for polβ wild-type, T304I, and DM mutants, respectively, and correspond to time points of 10, 30, 45, and 60 s. **(C)** Line 1 is the negative enzyme control of the one nucleotide gap DNA substrate. Lanes 2–5, 6–9 and 10–13 are the ligation of dGTP:C insertion products by LIGIIIα for polβ TM1, TM2, and DM/TM mutants, respectively, and correspond to time points of 10, 30, 45, and 60 s. **(D)** Graph shows time-dependent change in the amount of ligation products and the data represent the average of three independent experiments ± SD.

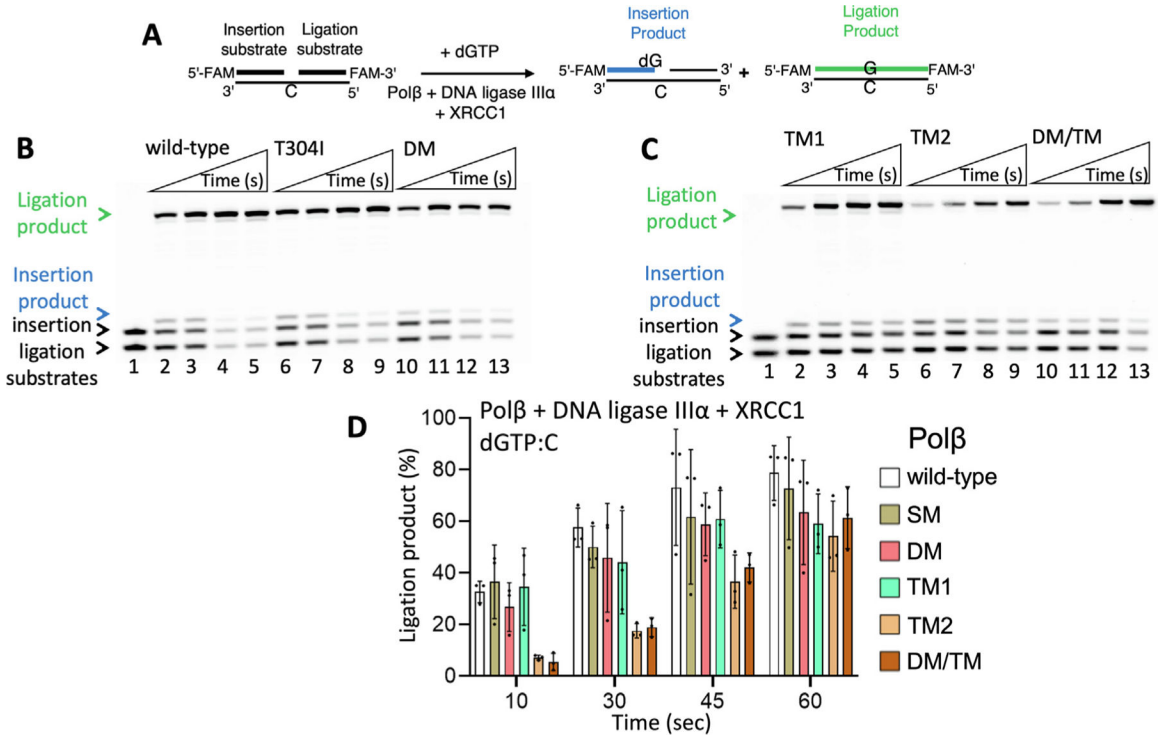

Figure 11. Impact of XRCC1 on the efficiency of ligation by DNA ligase IIIα after correct nucleotide insertion by polβ variants.

(A) Illustration of one nucleotide gap DNA substrate and the products of insertion and ligation in the coupled assays including polβ, XRCC1, LIGIIIα, and dGTP. **(B)** Line 1 is the negative enzyme control of the one nucleotide gap DNA substrate. Lanes 2–5, 6–9 and 10–13 are the ligation of dGTP:C insertion products by LIGIIIα in the presence of XRCC1 for polβ wild-type, T304I, and DM mutants, respectively, and correspond to time points of 10, 30, 45, and 60 s. **(C)** Line 1 is the negative enzyme control of the one nucleotide gap DNA substrate. Lanes 2–5, 6–9 and 10–13 are the ligation of dGTP:C insertion products by LIGIIIα in the presence of XRCC1 for polβ TM1, TM2, and DM/TM mutants, respectively, and correspond to time points of 10, 30, 45, and 60 s. **(D)** Graph shows time-dependent change in the amount of ligation products and the data represent the average of three independent experiments ± SD.

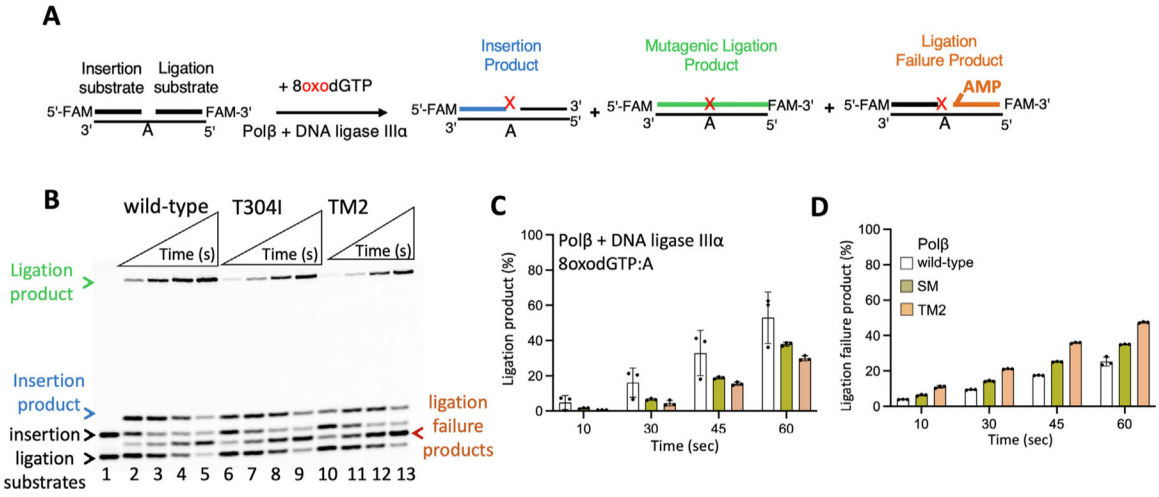

Figure 12. DNA ligase IIIα fails on nick repair product after oxidized nucleotide insertion by polβ variants.

(A) Illustration of one nucleotide gap DNA substrate and the products of insertion, ligation, and ligation failure in the coupled assays including polβ, DNA ligase IIIα, and 8oxodGTP. **(B)** Line 1 is the negative enzyme control of the one nucleotide gap DNA substrate. Lanes 2–5, 6–9 and 10–13 are the ligation of 8oxodGTP:A insertion products by LIGIIIα for polβ wild-type, SM, and TM2 mutants, respectively, and correspond to time points of 10, 30, 45, and 60 s. **(C-D)** Graphs show time-dependent change in the amount of ligation (C) and ligation failure (D) products. The data represent the average of three independent experiments ± SD.